


In-plane magnetic field effect on switching voltage and thermal stability in electric-field-controlled perpendicular magnetic tunnel junctions

Cite as: AIP Advances 6, 075014 (2016); <https://doi.org/10.1063/1.4959593>

Submitted: 19 January 2016 . Accepted: 12 July 2016 . Published Online: 19 July 2016

C. Grezes , A. Rojas Rozas, F. Ebrahimi, J. G. Alzate, X. Cai, J. A. Katine, J. Langer , B. Ocker , P. Khalili Amiri, and K. L. Wang



View Online



Export Citation



CrossMark

ARTICLES YOU MAY BE INTERESTED IN

Ultra-low switching energy and scaling in electric-field-controlled nanoscale magnetic tunnel junctions with high resistance-area product

Applied Physics Letters **108**, 012403 (2016); <https://doi.org/10.1063/1.4939446>

Enhancement of voltage-controlled magnetic anisotropy through precise control of Mg insertion thickness at CoFeB/MgO interface

Applied Physics Letters **110**, 052401 (2017); <https://doi.org/10.1063/1.4975160>

Electric field-induced magnetization reversal in a perpendicular-anisotropy CoFeB-MgO magnetic tunnel junction

Applied Physics Letters **101**, 122403 (2012); <https://doi.org/10.1063/1.4753816>

AIP Conference Proceedings
FLASH WINTER SALE!

50% OFF ALL PRINT PROCEEDINGS

ENTER CODE 50DEC19 AT CHECKOUT



In-plane magnetic field effect on switching voltage and thermal stability in electric-field-controlled perpendicular magnetic tunnel junctions

C. Grezes,^{1,a,b} A. Rojas Rozas,^{1,a} F. Ebrahimi,^{1,2} J. G. Alzate,¹ X. Cai,¹ J. A. Katine,³ J. Langer,⁴ B. Ocker,⁴ P. Khalili Amiri,^{1,2} and K. L. Wang¹

¹Department of Electrical Engineering, University of California, Los Angeles, California 90095, USA

²Inston Inc., Los Angeles, California 90024, USA

³HGST Inc., San Jose, California 95135, USA

⁴Singulus Technologies AG, Kahl am Main 63796, Germany

(Received 19 January 2016; accepted 12 July 2016; published online 19 July 2016)

The effect of in-plane magnetic field on switching voltage (V_{sw}) and thermal stability factor (Δ) are investigated in electric-field-controlled perpendicular magnetic tunnel junctions (p-MTJs). Dwell time measurements are used to determine the voltage dependence of the energy barrier height for various in-plane magnetic fields (H_{in}), and gain insight into the H_{in} dependent energy landscape. We find that both V_{sw} and Δ decrease with increasing H_{in} , with a dominant linear dependence. The results are reproduced by calculations based on a macrospin model while accounting for the modified magnetization configuration in the presence of an external magnetic field. © 2016 Author(s). All article content, except where otherwise noted, is licensed under a Creative Commons Attribution (CC BY) license (<http://creativecommons.org/licenses/by/4.0/>). [<http://dx.doi.org/10.1063/1.4959593>]

Magnetic tunnel junctions (MTJs) exploiting voltage-controlled magnetic anisotropy (VCMA) have attracted interest for use in memory applications,^{1–11} offering the potential for ultralow switching energy,^{5–8} while employing conventional material combinations of stable MTJs with high tunneling magnetoresistance (TMR) ratios. Nanosecond bidirectional magnetization switching by the application of unipolar voltage pulses has been demonstrated,^{1–4} and switching energy down to 6fJ/bit has been achieved in VCMA-controlled CoFeB/MgO magnetic tunnel junctions with perpendicular anisotropy (p-MTJs).¹¹ During the voltage pulse application, the two stable magnetization states of the free layer disappear in favor of in-plane easy axis and a precessional motion of the magnetization appears. The magnetization switching is achieved by timing of the pulse duration.

In practical situations however, an in-plane magnetic field (e.g. applied externally or provided by an in-plane fixed layer) is needed to ensure a single in-plane precessional axis,^{9–11} and hence modifies the energy landscape and switching behavior. The modification of the energy landscape affects the relevant parameters of the MTJs, including: (1) the thermal stability ($\Delta = E_b/k_B T$, where E_b denotes the energy barrier that separates the two magnetization states, k_B is the Boltzmann constant, and T is the temperature), which characterizes the ability of the magnetization states to remain stable against thermal fluctuations, (2) the switching voltage (V_{sw}), which corresponds to the voltage required to switch between the two magnetization configurations, and (3) the switching time, equal to half the precession period. Recently, the effect of in-plane magnetic field on the period of the magnetization precession was studied in p-MTJs.^{12,13} In this Letter, we investigate the dependence of thermal stability and switching voltage on in-plane magnetic fields (H_{in}). We first provide a method for measuring the voltage-dependent energy barrier height $E_b(V)$, and gain insight into the energy landscape. We then apply the above method combined with switching experiments

^aC. Grezes and A. Rojas Rozas contributed equally to this work.

^bAuthor to whom correspondence should be addressed. Electronic mail: grezes.cecile@gmail.com

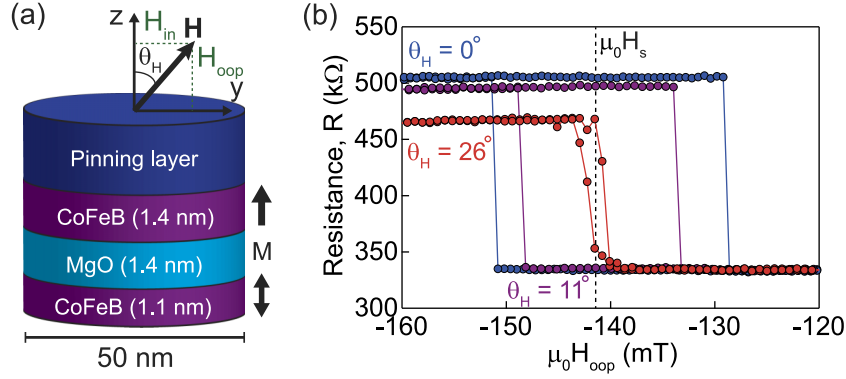


FIG. 1. (a) Schematic of the device structure and measurement configuration. An external magnetic field (\mathbf{H}) is applied at a tilted angle of θ_H from the film normal. H_{oop} (H_{in}) denotes the out-of-plane (in-plane) component of \mathbf{H} . (b) Tunnel magnetoresistance versus H_{oop} measured under +10 mV for $\theta_H = 0^\circ$, 11° , and 26° . The dashed line indicates the out-of-plane offset field ($\mu_0 H_s = -142$ mT) that compensates the stray field from the fixed layers.

to reveal the effect of in-plane magnetic fields on the energy landscape and related MTJs parameters. Our results indicate that both Δ and V_{sw} decrease with the increase of H_{in} , with a dominant linear dependence. These observations are accurately reproduced by calculations of the energy landscape based on a macrospin model.

A schematic of the MTJ and measurement configuration used in this study is shown in Figure 1(a). The stack structure consists of a bottom 1.1 nm (t) thick $\text{Co}_{20}\text{Fe}_{60}\text{B}_{20}$ free layer, a 1.4 nm (t_d) thick MgO barrier layer, and top 1.4 nm thick $\text{Co}_{20}\text{Fe}_{60}\text{B}_{20}$ reference layer with a synthetic antiferromagnetic pinning layer. This is the same structure as that used in Ref. 11. The film is processed into a circular MTJ of 50 nm (d) in junction diameter by using electron-beam lithography and dry etching techniques. Both CoFeB layers have perpendicular easy axes, and the magnetization direction of the CoFeB reference layer is fixed to the +z direction. A tilted external magnetic field (\mathbf{H}) is applied with an angle θ_H from the film normal. The out-of-plane (H_{oop}) and in-plane (H_{in}) components of \mathbf{H} correspond to $H \cos \theta_H$ and $H \sin \theta_H$, respectively.

Figure 1(b) shows measurements of resistance R as a function of the out-of-plane component of the magnetic field H_{oop} under +10 mV dc bias for $\theta_H = 0^\circ$, 11° , and 26° . The junction resistance-area product is $650 \Omega \cdot \mu\text{m}^2$, and the tunnel magnetoresistance ratio, defined as $(R_{AP} - R_P)/R_P$ at $\theta_H = 0^\circ$, is 49%, where R_P and R_{AP} are the resistances at parallel (P) and anti-parallel (AP) magnetization configurations, respectively. Increasing H_{in} is observed to decrease the coercivity of the free layer along the perpendicular axis, in agreement with previous studies in similar structures.^{12,13} The hysteresis curves are shifted at negative H_{oop} , due to stray fields from the fixed (i.e. combined pinning and reference) layers acting on the CoFeB free layer. The shift is found to be independent of θ_H , which indicates that the directions of magnetization in the fixed layers are not tilted from the sample normal during the experiment. Hereafter, we present and compare results for various H_{in} , where the out-of-plane component of \mathbf{H} is maintained near $\mu_0 H_{oop} = \mu_0 H_s = -142$ mT, to compensate the stray field. Values of E_b and V_{sw} are determined from $\mu_0 H_{oop}$ strictly fixed to $\mu_0 H_s$.

Energy barrier heights (E_b) are obtained by measuring the mean time for thermally activated switching (dwell time) under different applied magnetic fields.¹⁴ The mean value at a particular magnetic field is determined from a total of 10^2 switching events, which are monitored by measuring the real-time voltage across the MTJ (Figure 2(a)–2(b)). The dwell times from P to AP (τ^+) and AP to P (τ^-) are then fitted using the Neel-Brown formula,¹⁵

$$\tau^\pm = \tau_0 \exp \left(\frac{E_b}{k_B T} \left(1 \pm \frac{H_{oop} - H_s}{H_{k,eff}} \right)^2 \right), \quad (1)$$

where τ_0 is the inverse of the attempt frequency (assumed to be 1 ns), and $H_{k,eff}$ is the effective magnetic anisotropy field. In the following, we restrict our measurements to $E_b > 15 k_B T$ to remain

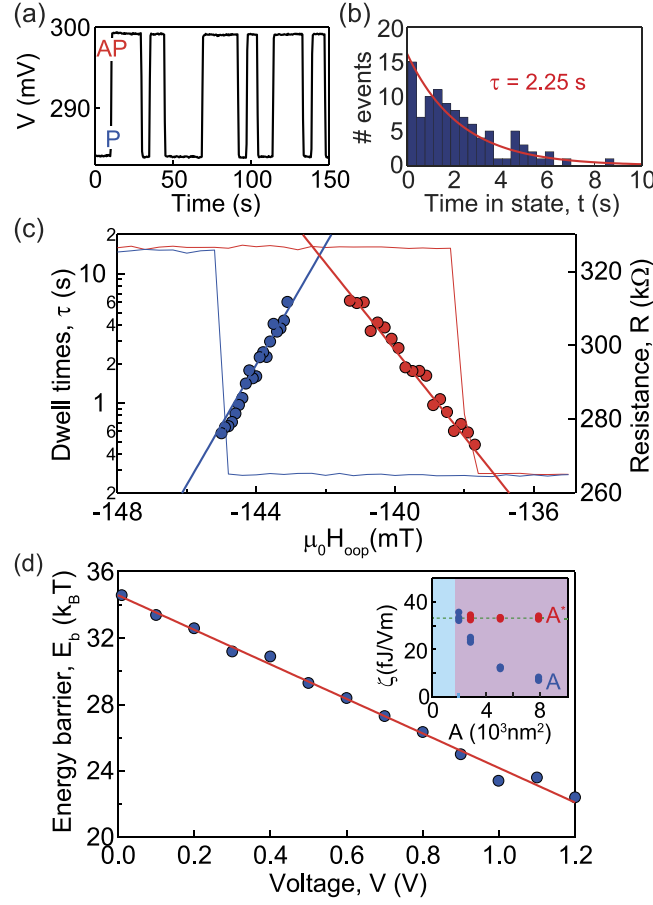


FIG. 2. Dwell time measurement results for $\theta_H = 0^\circ$ ($\mu_0 H_{in} = 0$ mT). (a) Real-time voltage measured at the scope for +1 V dc bias across the MTJ and $\mu_0 H_{oop} = \mu_0 H_s$. The device is incorporated into a voltage divider circuit. (b) Distribution for P state dwell times for +1 V dc bias and $\mu_0 H_{oop} = -143.9$ mT, fitted by an exponential envelope corresponding to a Poissonian distribution. (c) Tunnel magnetoresistance (referenced to the right axis) and dwell times (referenced to the left axis) from P to AP (blue) and AP to P (red) versus H_{oop} under +1 V dc bias. The fits (solid lines) using Eq. (1) yields a retention time $\tau = 13.9$ s, corresponding to an energy barrier height $E_b = 23.3$ k_BT. (d) Energy barrier E_b as a function of the dc bias voltage, yielding $\Delta = 34.6$ and $\xi = 30.5$ fJ $V^{-1}m^{-1}$ (red line is a fit to Eq. (3)). The inset shows the comparison between ξ fitted to Eq. (3) using the nominal junction area A (blue) and the sub-volume area A^* (red) for various junction size. The fit using A^* is in good agreement with ξ as determined by switching experiments (green), confirming the validity of the model both in the single-domain (blue) and nucleation reversal regimes (purple).

in the regime of high energy barriers ($E_b \gg k_B T$) in which Eq. (1) is valid.¹⁶ Figure 2(c) shows a typical result of dwell time measurements for $\mu_0 H_{in} = 0$ mT under +1 V dc bias. The measured dwell times are well fitted by Eq. (1), showing a symmetric behavior with respect to H_s . At $\mu_0 H_{oop} = \mu_0 H_s$, the relaxation times for the two states are equal $\tau^\pm = \tau = \tau_0 \exp(E_b/k_B T)$, and the energy barrier height $E_b = 23.3$ k_BT can be read directly at the intersection of the fits.

First, we focus on the voltage dependence of E_b in the absence of in-plane magnetic field. As shown in Figure 2(d), the energy barrier decreases linearly with positive voltage. This indicates a modulation of the perpendicular magnetic anisotropy by the applied voltage. The magnetic energy density S per unit volume is given by the sum of the densities of the Zeeman energy, demagnetizing energy, and magnetic anisotropy energy as

$$\begin{aligned}
 S &= K \sin^2 \theta + \frac{M_s^2}{2\mu_0} \cos^2 \theta - H_{in} M_s \sin \theta \\
 &= K_{eff} \sin^2 \theta - H_{in} M_s \sin \theta + \frac{M_s^2}{2\mu_0},
 \end{aligned} \tag{2}$$

where μ_0 is the permeability of vacuum, M_s is the free layer saturation magnetization, K is the first-order perpendicular magnetic anisotropy energy constant, and θ is the magnetization angle measured from the sample normal. We introduce the effective magnetic anisotropy energy $K_{\text{eff}} = \frac{M_s H_{k,\text{eff}}}{2} = K - \frac{M_s^2}{2\mu_0}$, which corresponds to the difference in the magnetic energy densities between $\theta = 0^\circ$ and $\theta = 90^\circ$ at zero magnetic field. Note that, a more detailed analysis should also include the second-order magnetic anisotropy term $K_2 \sin^4 \theta$. We neglect this in the following and find that this assumption adequately captures our experimental results, consistent with the recent experiments in CoFeB/MgO MTJs showing that K_2 is several time smaller than K .^{17,18} The energy barrier E_b can be calculated from Eq. (2) as the product of the difference between the maximum and minimum energy densities ΔS and the volume of the free layer $V^* = A^* t$ ($= t\pi(d/2)^2$ in the single domain case). In the absence of in-plane magnetic field, the maximum and minimum energy density for a perpendicular MTJ coincide with the hard ($\theta = 90^\circ$) and easy ($\theta = 0^\circ$) anisotropy axis, respectively, yielding $E_b(H_{\text{in}} = 0) = K_{\text{eff}} V^*$. Assuming a linear dependence of the first-order anisotropy energy on voltage,^{19,20} one can write K as $K(V) = (K_i - \frac{\xi}{t_d} V)/t$ (where K_i is the interfacial anisotropy energy density and ξ is the linear VCMA magnetoelectric coefficient) and express the voltage-dependent energy barrier (in the absence of in-plane magnetic field) as

$$E_b(H_{\text{in}} = 0) = E_{b,s} - \frac{\xi A^*}{t_d} V, \quad (3)$$

where $\Delta = E_{b,s}/k_B T = \left(K_i - \frac{M_s^2}{2\mu_0} t\right) A^*/k_B T$ is the standby thermal stability of the device. The fit to Eq. (3) yields $\Delta = 34.6$ and $\xi = 30.5 \text{ fJ V}^{-1} \text{ m}^{-1}$, with $K_i = 0.24 \text{ mJ m}^{-2}$ and $M_s = 0.616 \text{ T}$ (corresponding to a zero-voltage perpendicular anisotropy field $\mu_0 H_{k,\text{eff},0} = \mu_0 H_{k,\text{eff}}(V = 0) = 268 \text{ mT}$). Note that these values of K_i , M_s , $\mu_0 H_{k,\text{eff},0}$ and ξ should be taken as lower limits, since sub-volume nucleation may exist in the CoFeB free layer,^{21–23} and hence an overestimated free layer area A^* would serve to lower the apparent values (see inset). Noteworthy, in the absence of in-plane field, the critical voltage V_c , defined as the voltage required to reduce the energy barrier to zero ($E_b(V_c) = 0$), can be estimated straightforwardly by linear extrapolation of the measured voltage-dependent energy barrier height, yielding $V_c = 3.32 \text{ V}$.

Figure 3(a) shows the voltage dependence of the energy barrier height for various in-plane magnetic fields H_{in} . It is observed that E_b decreases (increases) linearly with increasing positive (negative) voltage, with a slope independent of H_{in} in the investigated region ($E_b > 15 k_B T$). This behavior can be explained by considering again Eq. (2). For non-zero in-plane magnetic field, the two stable magnetizations states are no longer along the easy anisotropy axis ($\theta = 0^\circ$), but tilted from the sample normal with an angle $\theta_3 = \sin^{-1}(H_{\text{in}}/H_{k,\text{eff}})$ and $\theta_4 = \pi - \sin^{-1}(H_{\text{in}}/H_{k,\text{eff}})$ (fixed by the energy minimum conditions, $\partial S/\partial \theta = 0$ and $\partial^2 S/\partial^2 \theta > 0$). The voltage-dependent energy barrier height $E_b = (S(\theta_{1,2}) - S(\theta_{3,4})) V^*$ (with $\theta_{1,2} = \pm 90^\circ$, along the hard anisotropy axis) becomes

$$E_b = \left(K_{\text{eff}} - H_{\text{in}} M_s + \frac{M_s^2}{4K_{\text{eff}}} H_{\text{in}}^2 \right) V^*, \quad (4)$$

with a third term $\frac{M_s^2}{4K_{\text{eff}}} H_{\text{in}}^2 V^*$ that results in nonlinearity both as a function of V and H_{in} . This non-linear term however is negligible when $\frac{M_s^2}{4K_{\text{eff}}} H_{\text{in}}^2 \ll K_{\text{eff}} H_{\text{in}} M_s$, conditions that reduce to $H_{\text{in}} \ll H_{k,\text{eff}}$. In the experimental data shown in Figure 3, the condition $H_{\text{in}} \ll H_{k,\text{eff}}$ is always satisfied since we restrict our measurements to the regime where $E_b > 15 k_B T$ (as also shown below in Figure 5). The corresponding zero-voltage energy barrier height $E_{b,0}$ and VCMA coefficient ξ as a function of H_{in} are shown in Figure 3(b). It is observed that $E_{b,0}$ decreases almost linearly with H_{in} , a result well described by Eq. (4) for zero-voltage

$$E_{b,0} = E_{b,s} - H_{\text{in}} M_s V^* + (H_{\text{in}} M_s V^*/2)^2 / E_{b,s}, \quad (5)$$

using the same values of $E_{b,s}$, M_s and V^* as in Eq. (3) (dashed-dotted line). This indicates that the nonlinearity in H_{in} arising from the third term in Eq. (5) is small, as expected for $\mu_0 H_{\text{in}} \leq 102 \text{ mT} \ll \mu_0 H_{k,\text{eff},0}$. We note that Eq. (5) is independent of the switching mechanism used during writing,

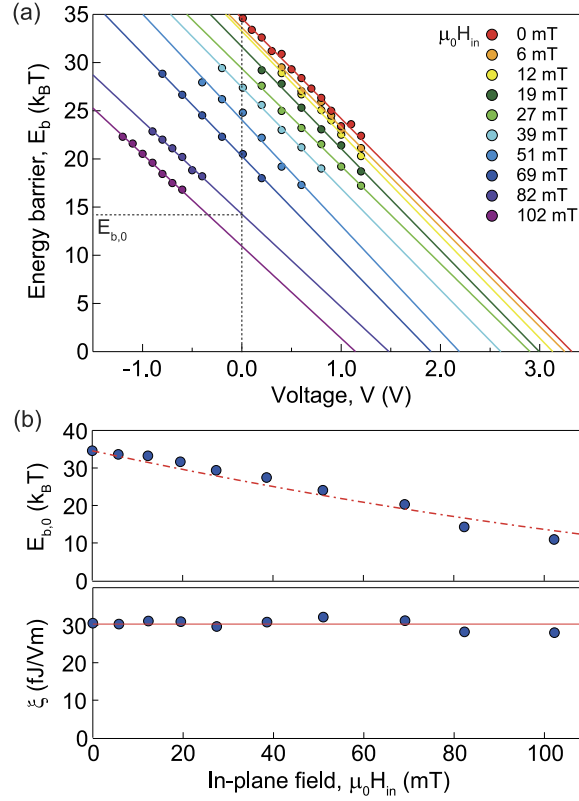


FIG. 3. (a) Voltage dependence of the energy barrier height for various applied in-plane magnetic field. Solid lines correspond to linear fits. (b) Corresponding (dots) $E_{b,0}$ and ξ as a function of H_{in} . The red dashed-dotted line is the result of calculations using Eq. (5).

hence the above conclusions extend straightforwardly to field-driven and spin-transfer torque driven pMTJs. The VCMA coefficient, extracted from the slope as $E_b = E_{b,0} - \frac{\xi A^*}{t_d} V$, is found to be constant at $30 \text{ fJ V}^{-1} \text{ m}^{-1}$, confirming that the condition of negligible nonlinearity $H_{in} \ll H_{k,eff}$ is also satisfied for non-zero voltage.

We focus now on the in-plane magnetic field dependence of the switching voltage. One can see in Figure 3(a) that the voltage at which the energy barrier is reduced to zero decreases with increasing H_{in} . In order to estimate this threshold, we performed electric-field induced switching measurements using voltage pulses of various lengths (t_{pulse}) and amplitudes (V_{pulse}) applied to the device. The measurement setup and procedure are identical to the ones of our previous study (Ref. 11), and the switching probability precision is 0.05. Figure 4(a) shows the measured back and forth magnetization switching ($P_{01}P_{10}$) by two successive 1.9 V voltage pulses, as functions of pulse duration and out-of-plane (in-plane) component of the external magnetic field. The quantity $P_{01}P_{10}$ corresponds to the product of the probabilities of P to AP transition (P_{10}) and AP to P transition (P_{01}). An oscillatory dependence of the switching probability on the pulse duration is observed for the range of H_{in} investigated, which is a signature of the voltage-induced precessional motion of the magnetization. The period of the oscillations is seen to decrease with the increase of H_{in} magnitude. This indicates a reduction of the Larmor frequency with H_{in} , in good agreement with previous studies in similar voltage-controlled MTJs.^{12,13} The switching voltage is obtained by measuring the contrast of the first oscillation as a function of the pulse amplitude. To allow a comparison with the simulations, we introduce the threshold (switching) voltage V_{sw} at which the contrast exceed 50% ($P_{01}P_{10} > 0.25$), the maximum switching errors induced by thermal fluctuations. Note that this definition does not necessarily correspond to the precessional critical voltage V_c as defined by $E_b(V_c) = 0$ since switching can occur also below V_c by thermal activation across the energy barrier

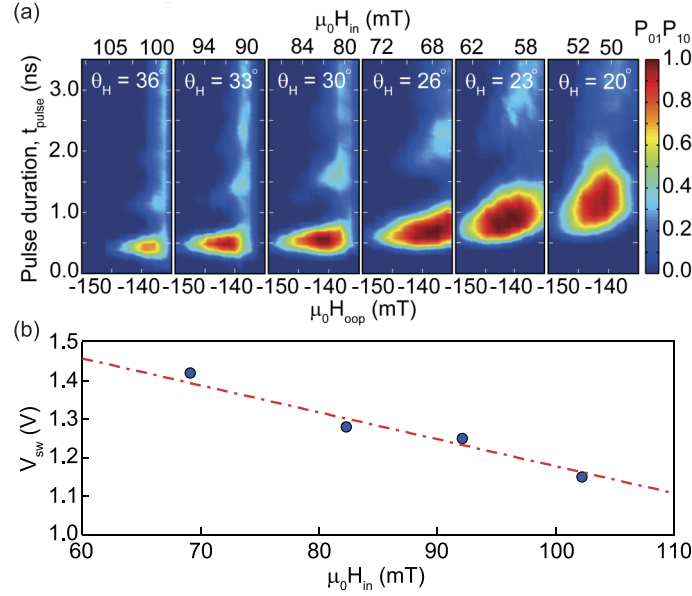


FIG. 4. (a) Measured switching probabilities of back and forth magnetization switching ($P_{01}P_{10}$) by two successive 1.9 V voltage pulses as functions of pulse duration for various external magnetic field angle θ_H , and $\mu_0 H_{\text{oop}} = [-150, -135]$ mT. Corresponding in-plane component of external magnetic field is shown on the top axis. (b) Measured V_{sw} as a function of H_{in} . The red dashed-dotted line is the results of simulations using Eq. (4), rescaled to account for the difference of definition between the measured V_{sw} and simulated V_c .

during voltage pulse applications.²⁴ The measured V_{sw} for $\mu_0 H_{\text{in}} = 69, 82, 92$ and 102 mT is shown in Figure 4(b). Its dependence on H_{in} is well reproduced by the simulations of V_c , obtained by resolving numerically the equation $E_b(V_c) = 0$, where E_b is given by Eq. (4).

In order to gain insight into the observed experimental characteristics, we show in Figure 5 the results of the calculations with our experimental parameters. The energy landscape in Figure 5(a) is obtained by calculating the magnetic energy SV^* of the CoFeB free layer from Eq. (2) for a set of magnetization angles θ and in-plane fields H_{in} . The stable magnetization states are observed to be shifted towards the hard anisotropy axis ($\theta = 90^\circ$) with increasing H_{in} (white dashed-lines). For $H_{\text{in}} > H_{k,\text{eff},0}$, the easy axis is aligned with the direction of H_{in} (fully in-plane). Figure 5(b) shows the voltage dependence of the energy barrier height for various H_{in} values as determined from Eq. (4). The macrospin model reproduces quantitatively our experimental results shown in Figure 3(a). The remaining small discrepancy could be attributed to the effect of the second-order

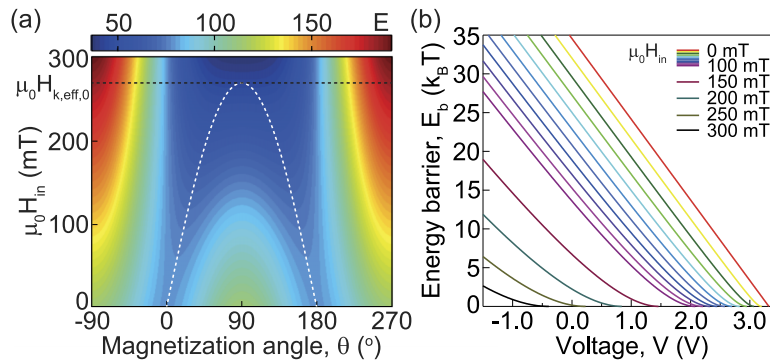


FIG. 5. (a) Calculated energy landscape (in unit of $K_B T$) as a function of the magnetization angle θ and magnitude of the in-plane magnetic field. The white dashed-lines indicate the energy minima. The zero-voltage perpendicular anisotropy field $\mu_0 H_{k,\text{eff},0}$ is shown as a black dashed-line. (b) Calculated voltage dependence of the energy barrier height for various H_{in} .

anisotropy and nonuniformity of the magnetization profile. Further study is needed to precisely understand the contributions of the higher order anisotropy in canted magnetization states and develop improved VCMA-based MTJs.²⁵

In conclusion, we have investigated the dependence of switching voltage and thermal stability on in-plane magnetic field in electric-field-controlled CoFeB/MgO perpendicular magnetic tunnel junctions. Both switching voltage and thermal stability factor decrease with the increase of in-plane magnetic field, with a behavior dominated by a linear dependence for $H_{in} \ll H_{k,eff,0}$. These results are accurately reproduced by calculations based on a macrospin model, which indicates a tuning with H_{in} of the stable magnetization states towards the hard anisotropy axis.

This work was partially supported by the National Science Foundation Nanosystems Engineering Research Center for Translational Applications of Nanoscale Multiferroic Systems (TANMS). The work at Inston Inc. was supported in part by a Phase II NSF Small Business Innovation Research award. We would also like to acknowledge the collaboration of this research with King Abdul-Aziz City for Science and Technology (KACST) via The Center of Excellence for Green Nanotechnologies (CEGN). The authors would like to thank the members of the UCLA Device Research Laboratory, TANMS, CEGN and Inston Inc. for fruitful discussions.

- ¹ W. G. Wang, M. Li, S. Hageman, and C. L. Chien, *Nat. Mater.* **11**(1), 64 (2012).
- ² Y. Shiota, T. Nozaki, F. Bonell, S. Murakami, T. Shinjo, and Y. Suzuki, *Nat. Mater.* **11**(1), 39 (2012).
- ³ J. G. Alzate, P. K. Amiri, P. Upadhyaya, S. S. Cherepov, J. Zhu, M. Lewis, R. Dorrance, J. A. Katine, J. Langer, K. Galatsis, D. Markovic, I. Krivorotov, and K. L. Wang, 2012 IEEE International Electron Devices Meeting (2012).
- ⁴ S. Kanai, M. Yamanouchi, S. Ikeda, Y. Nakatani, F. Matsukura, and H. Ohno, *Appl. Phys. Lett.* **101**(12), 122403 (2012).
- ⁵ K. L. Wang and P. Khalili Amiri, *SPIN* **02**(03), 1240002 (2012).
- ⁶ K. L. Wang, J. G. Alzate, and P. Khalili Amiri, *Journal of Physics D: Appl. Phys.* **46**(7), 074003 (2013).
- ⁷ P. Khalili Amiri, J. Alzate, X. Cai, F. Ebrahimi, Q. Hu, K. Wong, C. Grezes, H. Lee, G. Yu, X. Li, M. Akyol, Q. Shao, J. Katine, J. Langer, and B. Ocker, *Magnetics, IEEE Transactions on Magnetics* (99), 1 (2015).
- ⁸ P. Khalili Amiri and K. L. Wang, *IEEE Spectrum* **52**(7), 30 (2015).
- ⁹ Y. Shiota, S. Miwa, T. Nozaki, F. Bonell, N. Mizuochi, T. Shinjo, H. Kubota, S. Yuasa, and Y. Suzuki, *Applied Physics Letters* **101**, 102406 (2012).
- ¹⁰ W. G. Wang and C. L. Chien, *J. Phys. D: Appl. Phys.* **46**, 074004 (2013).
- ¹¹ C. Grezes, F. Ebrahimi, J. G. Alzate, X. Cai, J. A. Katine, J. Langer, B. Ocker, P. Khalili Amiri, and K. L. Wang, *Appl. Phys. Lett.* **108**, 012403 (2016).
- ¹² S. Kanai, Y. Nakatani, M. Yamanouchi, S. Ikeda, F. Matsukura, and H. Ohno, *Appl. Phys. Lett.* **103**, 072408 (2013).
- ¹³ S. Kanai, M. Yamanouchi, S. Ikeda, Y. Nakatani, F. Matsukura, and H. Ohno, *IEEE Transactions on Magnetics* (50), 1 (2014).
- ¹⁴ W. Rippard, R. Heindl, M. Pufall, S. Russek, and A. Kos, *Phys. Rev. B* **84**, 064439 (2011).
- ¹⁵ W. F. Brown, Jr., *Phys. Rev.* **130**, 1677 (1963).
- ¹⁶ Z. Li and S. Zhang, *Phys. Rev. B* **69**, 134416 (2004).
- ¹⁷ K. Mizunuma, M. Yamanouchi, H. Sato, S. Ikeda, S. Kanai, F. Matsukura, and H. Ohno, *Appl. Phys. Express* **6**, 063002 (2013).
- ¹⁸ A. Okada, S. Kanai, M. Yamanouchi, S. Ikeda, F. Matsukura, and H. Ohno, *Appl. Phys. Lett.* **105**, 052415 (2014).
- ¹⁹ T. Nozaki, Y. Shiota, M. Shiraishi, T. Shinjo, and Y. Suzuki, *Appl. Phys. Lett.* **96**, 022506 (2010).
- ²⁰ J. Zhu, J. A. Katine, G. E. Rowlands, Y. Chen, Z. Duan, J. G. Alzate, P. Upadhyaya, J. Langer, P. Khalili Amiri, K. L. Wang, and I. N. Krivorotov, *Phys. Rev. Lett.* **108**, 197203 (2012).
- ²¹ J. Z. Sun, R. P. Robertazzi, J. Nowak, P. L. Trouilloud, G. Hu, D. W. Abraham, M. C. Gaidis, S. L. Brown, E. J. O'Sullivan, W. J. Gallagher, and D. C. Worledge, *Phys. Rev. B* **84**, 064413 (2011).
- ²² H. Sato, M. Yamanouchi, K. Miura, S. Ikeda, H. D. Gan, K. Mizunuma, R. Koizumi, F. Matsukura, and H. Ohno, *Appl. Phys. Lett.* **99**, 042501 (2011).
- ²³ H. Sato, E. C. I. Enobio, M. Yamanouchi, S. Ikeda, S. Fukami, S. Kanai, F. Matsukura, and H. Ohno, *Appl. Phys. Lett.* **105**, 062403 (2014).
- ²⁴ P. Khalili Amiri, P. Upadhyaya, J. G. Alzate, and K. L. Wang, *J. Appl. Phys.* **113**, 013912 (2013).
- ²⁵ Y. Shiota, T. Nozaki, S. Tamaru, K. Yakushiji, H. Kubota, A. Fukushima, S. Yuasa, and Y. Suzuki, *Appl. Phys. Exp.* **9**, 1 (2015).